Wave Inversion Technology, Report No. 2, pages 179-186

Numerical modeling of borehole effects in cross-well seismics

J. Falk, E. Teßmer and D. Gajewski[1]

keywords: *cross-well, wave scattering, seismic modeling, finite-difference, adapted grids*

ABSTRACT

Wave propagation simulations of cross-well configurations commonly neglect the influences of both the source well and the receiver well on the wavefield recordings. This is due to the fact that the modeling methods can not resolve two boreholes within complex subsurface structures. Recent developments in finite-difference seismic forward modeling overcome these restrictions. Grid refinement techniques are applied in order to combine two different scales, the scale related to the size of the boreholes and the scale related to the wavelengths commonly present in cross-well experiments.
Our numerical study shows that for correct interpretation of cross-well recordings one has to consider very complex phenomena of wave scattering due to the presence of the boreholes. There are strong events related to tube wave scattering at the source well as well as tube wave generation due to the scattering of body waves and guided waves at the receiver well.

INTRODUCTION

Field data sets like cross-well measurements contain much more information than just primaries used for cross-well tomography. The increasing interest of exploration geophysicists in full waveform analysis encourages the research on modeling tools which are able to take into account subsurface models of high complexity. If we focus on full waveform modeling of borehole environments, nowadays there are commonly two different approaches used, boundary element methods, e.g., Bouchon and Schmitt (1989), Bouchon (1993), Dong et al. (1995a), Dong and Toksöz (1995b), and grid methods like the finite-difference (FD) method, e.g., Yoon and McMechan (1992), Cheng (1994). Grid methods generally resolve more complex subsurface structure models.
The FD methods are commonly based on equidistantly spaced staggered grids, e.g.,

[1]**email:** falk@dkrz.de (now j.falk@ta.tudelft.nl)

Virieux (1986). Because of the small scale of the borehole radius also the grid spacing must be chosen at a small scale. This restricts the applicability of the FD method based on equidistantly spaced grids to the modeling of high frequency borehole synthetics (sonic log simulations). The method proposed here extends the conventional FD method with respect to the applicability to the modeling of low frequency borehole seismic data like synthetic cross-well sections or VSP sections. The limitations due to the small scale in the borehole vicinity can be overcome by the application of grid refinement techniques. We refer to Fornberg (1988) and Jastram and Tessmer (1994) in order to explain the grid mapping method which has been used for our code in more detail. Such techniques enable the variation of the grid spacing by large factors within a transition zone between grid domains of fine and coarse regular spacing.
In the following we briefly review the grid mapping method. A 3-D modeling example is discussed to explain the complex wave scattering phenomena occurring in cross-well measurements even for very simple subsurface structures.

EXAMPLE

In the example we study the complex phenomena of wavefield scattering due to the presence of fluid-filled cylindrical boreholes in cross-well configurations. The front panel of the Figure 1 shows the model of a source well penetrating a thin dipping low-velocity layer like a fault zone filled with fault gouge. The sketch is given in the $x-z$-plane with y chosen at the borehole axes. The axes are aligned with the z-direction. The receiver well is located at 24.5 m distance in the dip direction of the layer. The layer thickness is h=2.4 m. The formation parameters are v_p=3000 m/s, v_s=1963 m/s and ρ=2.7 g/cm^3. The layer parameters are v_{p_l}=3000 m/s, v_{s_l}=1500 m/s and ρ_l=1.6 g/cm^3. Both wells are fluid-filled (v_{p_f}=1500 m/s, v_{s_f}=0 m/s and ρ_f=1.0 g/cm^3). The radius is R=0.15 m for both wells, respectively. This yields a large difference in scale between the borehole size and the wavelength of the *S*-wave in the embedding which is of the order of approximately 10 m. The top panel of Figure 1 schematically outlines the grid spacing in the horizontal directions *x* and *y*, respectively. The grid spacing has been refined towards the borehole locations in order to take into account the very small scale. Grid spacing varies between Δx=Δy=0.9 m within the coarsely sampled grid domains and Δx=Δy=$\frac{1}{60}$ 0.9 m = 1.5 cm in the finely sampled grid domains where the boreholes are defined. The vertical grid spacing is Δz=0.6 m throughout the grid. Using such a Cartesian grid obviously results in some staircase approximation of the borehole wall which is still accurate if the radius is approximated by a sufficient number of grid points. The entire mesh consists of $NX \times NY \times NZ = 166 \times 72 \times 121$ grid points. A single force point source is clamped at the borehole wall 9.6 m above the layer. Receivers record the pressure at the center of the receiver well. Computations are performed by a staggered grid FD scheme which is 6th order accurate in space and 2nd order in time. Within the finely sampled grid domain we reduce the spatial

approximation to 2nd order. The time step size counts Δt=2·10^{-6} s. A maximum propagation time of t=0.05 s then requires 25000 iteration cycles. The computations have been performed on a Cray J90 vector machine using a single CPU. One run took about 50 hours CPU-time. The computational effort can be reduced drastically to about 33 percent by the application of locally adjustable time step sizes Falk et al. (1998b). Figure 2 shows 4 snapshots of the vertical displacement component for a 2-D plane in the *x*-*z*-plane for *y* chosen at the center of the boreholes. We can observe a high energetic tube wave propagating downwards in the source well. The tube wave becomes partly scattered and transmitted at the low-velocity layer. The transmitted tube wave becomes partly reflected and scattered at the bottom of the source well. The reflected part is partly scattered again at the low-velocity layer. This results (at least) in three strong secondary wavefields radiated from the source well. In particular we observe tube wave to shear wave scattering. These shear wave events denoted by a,b and c are partly guided in the dipping layer. They become again scattered at the point of intersection of the layer and the receiver well. Three tube wave events related to this "re-scattering" (denoted by A, B, C) are generated in the receiver well disturbing the recordings of the body waves (Figure 3). The interpretation of the wave scattering phenomena is sketched in Figure 4. More complex subsurface structure models, containing more then two boreholes for instance, certainly result in much more complex wave scattering phenomena in cross-well configurations.

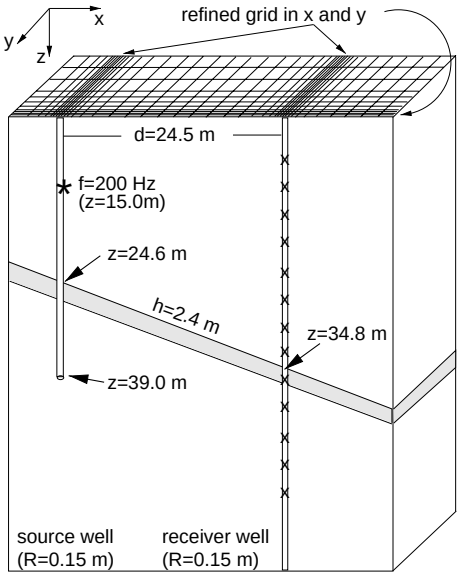

Figure 1: Simple cross-well configuration with a receiver well in direction of the dip of a thin low-velocity layer (e.g., a fault). The front panel shows the *x*-*z*-plane whereby *y* is taken as the well axes. The top panel outlines schematically that the horizontal grid spacing is variable in order to combine different scales related to the wavelengths (large scale) and related to the borehole radius (small scale).

CONCLUSIONS

We have presented a 3-D seismic modeling scheme based on the staggered grid FD approximation. The method enables the use of variable grid spacing to bridge the gap between different scales related to the borehole size and to the wavelengths present in

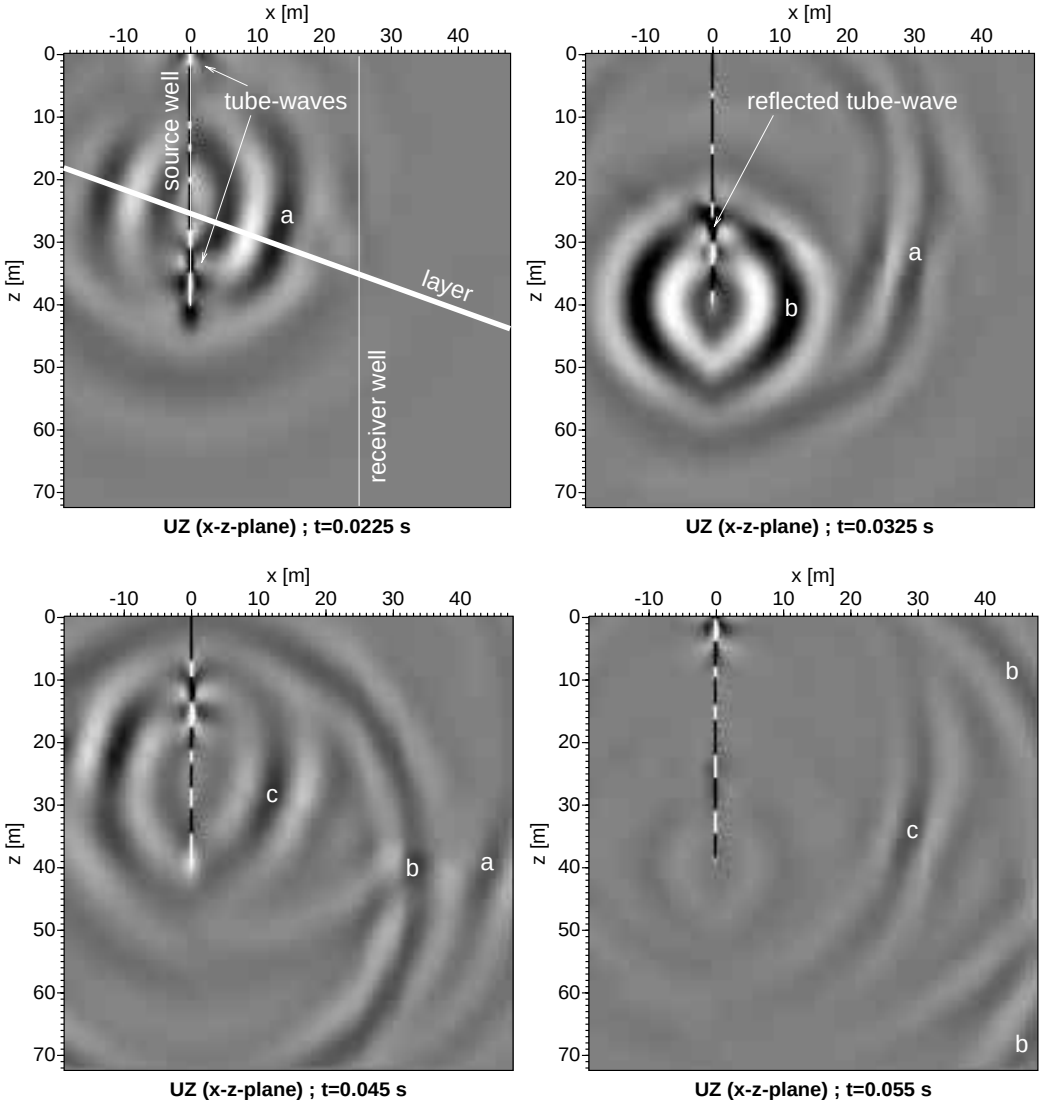

Figure 2: Four snapshots of the vertical displacement component. Three different secondary wavefields (*S*-waves) denoted by a,b and c are clearly observed. These events have been generated by tube wave scattering at the source well. a and c originate at the intersection of the borehole with the low-velocity layer but b is originated at the bottom of the source well. The snapshots have been re-sampled to equidistant spacings (Δx=38 cm ; Δz=40 cm).

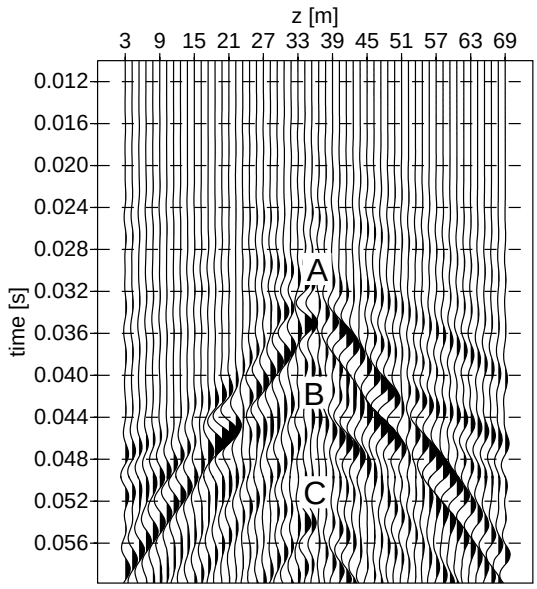

Figure 3: The secondary wavefields generated by tube wave scattering at the source well generate tube waves in the receiver well interfering with recordings of the body waves. Primaries are not observable at this amplitude scaling.

low frequency borehole seismics. An example of a synthetic cross-well configuration shows that complex phenomena of tube wave scattering and tube wave generation related to the presence of the boreholes have to be considered in the interpretation of cross-well data.

ACKNOWLEDGMENTS

The work was partly supported by the German Research Foundation DFG (Project Te 266/1-1) and by the Commission of the European Communities in the framework of the Joule II Programme (contract JOU2-CT92-0096) as well as by the WIT consortium.

Publications: Detailed results were published by Falk (1998) and Falk et al. (1998a).

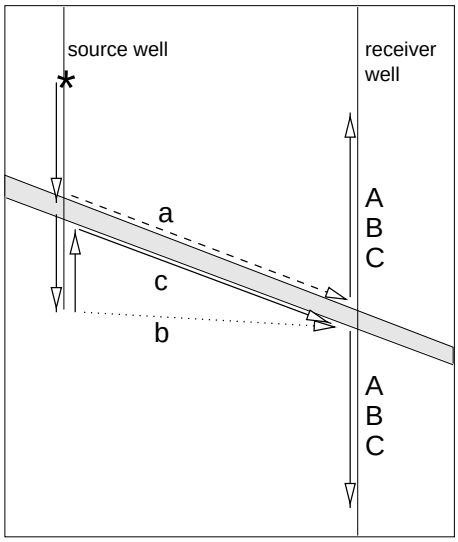

Figure 4: Tube wave generation at the receiver well (schematically). a,b and c denote *S*-waves generated by tube wave scattering at the source well. a: tube wave in the source well is partly scattered at the intersection with the layer. This yields a shear-wave propagating towards the receiver well. It becomes "re-scattered" at the receiver well inducing a tube wave A. b: shear wave generated by the tube wave scattering at the bottom of the source well. This shear wave becomes scattered at the receiver well generating the tube wave B. c: shear wave generated by scattering of the upwards traveling tube wave at the intersection with the layer. This shear wave becomes scattered at the receiver well generating the tube wave C.

REFERENCES

Bouchon, M., and Schmitt, D., 1989, Full-wave acoustic logging in an irregular borehole: Geophysics, **54**, 758–765.

Bouchon, M., 1993, A numerical simulation of the acoustic and the elastic wavefields radiated by a source in a fluid-filled borehole embedded in a layered medium: Geophysics, **58**, 475–481.

Cheng, N., 1994, Borehole Wave Propagation in Isotropic and Anisotropic Media: Three-Dimensional Finite Difference Approach: Ph.D. thesis, Massachusets Institute of Technology.

Dong, W., and Toksöz, M., 1995b, Borehole seismic-source radiation in layered isotropic and anisotropic media: Real data analysis: Geophysics, **60**, 748–757.

Dong, W., Bouchon, M., and Toksöz, M., 1995a, Borehole seismic-source radiation in layered isotropic and anisotropic media: Boundary element modeling: Geophysics, **60**, 735–747.

Falk, J., Tessmer, E., and Gajewski, D., 1998a, 3-D cross-well seismic modeling including the generation and scattering of tube waves: 68th Ann. Internat. Mtg., Soc. Expl. Geophys., Expanded Abstracts.

Falk, J., Tessmer, E., and Gajewski, D., 1998b, Efficient Finite-Difference Modelling of Seismic Waves Using Locally Adjustable Time Steps: Geophysical Prospecting, **in press**.

Falk, J., 1998, Efficient seismic modeling of small-scale inhomogeneities by the finite-difference method: Ph.D. thesis, University of Hamburg, Shaker Publishing B.V., ISBN90-423- 0062-0.

Fornberg, B., 1988a, Generation of finite difference formulas on arbitrarily spaced grids: Mathematics of Computation, **51**, 699–706.

Jastram, C., and Tessmer, E., 1994, Elastic modelling on a grid with vertically varying spacings: Geophysical Prospecting, **42**, 357–370.

Virieux, J., 1986, P-SV wave propagation in heterogeneous media velocity-stress finite-difference method: Geophysics, **51**, 889–901.

Yoon, K., and McMechan, G., 1992, 3-D finite-difference modelling of elastic waves in borehole environments: Geophysics, **57**, 793–804.